

Numerical Verification on a Countermeasure for High Level Sound Generated from Boiler Tube Bank Duct Using Walls Made of Perforated Plate and Cavity

Masaaki Mori¹, Takayuki Masumoto², Kunihiko Ishihara³
^{1,2}Cybernet Systems CO., LTD

³Department of Health and Welfare, Tokushima Bunri University

(¹m-mori@cybernet.co.jp, ²masumoto@cybernet.co.jp, ³k-ishihara@fe.bunri-u.ac.jp)

Abstract- Heat exchangers and boilers are widely used in various plants such as power plants and chemical plants. In the heat exchanger and the boiler, the tube bank is set in a duct, water passes through the inside of the tube, and gas flows the outside of the tube. Due to the external flow around tube banks, the resonance phenomenon called the self-sustained tone occurs at a certain velocity. The self-sustained tone might cause noise problems in the surroundings, cause losses due to plant shutdown, etc. In general, baffle plates are used to suppress the self-sustained tone. However, it is difficult to use them effectively, because appropriate insertion positions have not been established. On the other hand, to suppress the self-sustained tones, a method using perforated plates has been proposed. In this method, perforated plates were installed on both sides of the duct to suppress the self-sustained tones. The perforated plate has an acoustic damping and a resonance mode of the duct transverse direction to the flow is suppressed by its damping effect, when the self-sustained tone occurs.

The purpose of this study is to verify the effect of the perforated plates on the self-sustained tone numerically. CFD and acoustic simulations were carried out to examine the suppression effect of the perforated plates installed, and compared with the measurement data. The results show that the suppression effect appeared in all aperture ratio $\phi \Rightarrow 0.01(1\%)$ of the perforated plate and that the measurement and simulation data are in reasonable agreement in terms of prediction of effects of perforated plates on the self-sustained tones.

Keywords- *Self-Sustained Tone, Acoustic Resonance, Lock-in Phenomenon, Perforated Plate, CFD and BEM*

I. INTRODUCTION

Heat exchangers and boilers are widely used in various plants such as power plants and chemical plants. In heat exchangers such as boilers and gas heaters, tube banks are set in a duct, and water passes through the inside of the tube and warm gas passes through the outside of the tube. When the flow velocity increases, Karman vortex shedding occurs behind

the tubes. The vortex shedding frequency is proportional to the velocity. On the other hand, the duct has an acoustic natural frequency determined by the duct size and the sound speed. The acoustic natural frequency is independent of the flow velocity. A resonance phenomenon occurs at a certain velocity when the vortex shedding and acoustic natural frequencies coincide. Many studies on the excitation mechanisms of the acoustic resonance in the tube bank have been done [1, 2, 3, 4, 5, 6, 7, 8, 9]. Ziada and Oengören [10] have shown that vortex excitation results from the formation of periodic vortices in the space between tubes by visualization experiments in the waterway. Hamakawa et al. [11] focused on effect of arrangement of tube banks, and investigated the characteristics of vortex shedding and acoustic resonance from in-line and staggered tube banks.

It is generally known that the vortex shedding frequency suddenly locks on to the acoustic natural frequency of the duct when the flow velocity increases. This is a lock-in (lock-on) phenomenon. Fig. 1 shows the relation between frequency and velocity in a Lock-in phenomenon. When a lock-in phenomenon occurs, a high level of sound is generated and its generation mechanism is called self-sustained tone [12, 13]. The self-sustained tone might cause noise problems, and also cause plant shutdown and hence production losses, etc. In a lock-in phenomenon, as shown in Fig. 1, the frequency slightly rises as the flow velocity increases. Furthermore, when the acoustic damping of the sound field in the duct is large, the lock-in phenomenon occurs at a certain flow velocity and does not occur thereafter as the flow velocity increases. However, when the acoustic damping is small, a high level sound continues with increasing flow velocity, and the sound pressure level remains substantially constant [13]. This is due to the fact that when the shedding frequency of the Karman vortex generated as the gas passes through the tube bank and the acoustic resonance frequency of the duct are close to each other, the interior sound field in the duct is strongly excited and the strong vortices those has a shedding frequency matching the resonance frequency in the duct width direction are generated. As a result, the sound field is further excited in the duct. It is known that this phenomenon is caused by a self-excited mechanism. Also, Mohany et al focused on the self-

excited acoustic resonance of two side-by-side cylinders in a duct, and investigated the mechanism of the self-excited acoustic resonance by experiments and numerical solutions [14]. They have found that dynamic lift fluctuation on the cylinders and strong in-phase vortex shedding synchronization are generated by the acoustic resonance. In our previous work [15], we have performed numerical simulations of high level sound generated from tube bank duct and an acoustic simulation for a practical generation prediction of a self-sustained tone, and the simulation results showed the reasonable agreement with the experiments in terms of the generation prediction of the self-sustained tone. Thus, the self-sustained tone has been studied and the generation mechanism has been experimentally and numerically clarified.

For a countermeasure of the self-sustained tone, a method of inserting a partition plate called a baffle plate inside the duct is generally used. In this method, there is an effect to increase the natural frequency of the duct, detune the frequency of the vortex shedding from the tube bank and the acoustic natural frequency of the duct, and suppress the resonance phenomenon [16, 17, 18]. However, it has been reported that the natural frequency of the duct decreases by inserting the baffle plate [12], and it is not easy to decide an appropriate insertion position of the baffle plate. Hamakawa et al. [18] have investigated the effect of the baffle plate on the acoustic resonance generation from in-line tube banks with small cavity, and they found that although sound pressure level of an acoustic mode perpendicular to the flow (lift mode) is suppressed by a baffle plate, that of an acoustic mode parallel to the flow (drag mode) increases. On the other hand, to suppress the self-sustained tones, a method using perforated plates and cavities have been proposed by Ishihara and Nakaoka [13]. A perforated plate has long been used in various noise control applications, such as vehicle, exhaust systems, ducts, hearing protection devices, and acoustic panels, because it is well known that perforated plates has an acoustic damping effect [19, 20, 21, 22, 23]. Ishihara and Nakaoka [13] thought that a resonance mode of the duct transverse direction to the flow might be suppressed by a damping effect of perforated plates, when the self-sustained tone occurred. They carried out some experiments to examine the suppression effect of the perforated plates and cavities installed, and confirmed the suppression effect. They defined the aperture ratio ϕ of the perforated plate and investigated how the change in the value of the aperture ratio ϕ of the perforated plate affects the self-sustained tone in the duct. They varied the value of the aperture ratio ϕ from 1% to 32%. Further, Ishihara [24] clarified experimentally the critical and optimum aperture ratios, and the effect of a cavity volume which is used with perforated plates on the SPL. The results show that the critical aperture ratio is about 0.25% and the influence of the cavity volume on SPL is a little. The optimum aperture ratio is concluded to be 4%.

The purpose of this study is to verify the effect of the perforated plates on the self-sustained tone numerically. We define the aperture ratio of the perforated plate as in the experiments [13, 24], and clarify how the change in the value of the aperture ratio ϕ of the perforated plate affects the self-sustained tone in the duct. We perform compressible CFD and

acoustic simulations to verify the effect of the aperture ratio of the perforated plate on the self-sustained tone and acoustic resonance frequencies, and compare the simulation results with the measurements [13, 24].

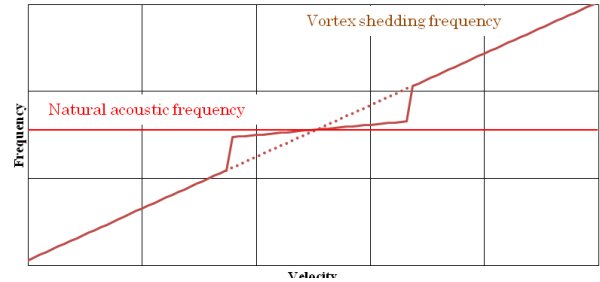


Figure 1. Relation between frequency and velocity in the case of Lock-in phenomenon.

II. EXPERIMENT

A. Experimental Setup

In this paper, we perform the CFD and acoustic simulations of the self-sustained tone and the suppression of the self-sustained tone using the perforated plate, and compare the simulation results with the measurements [13, 24]. In this chapter, we describe the experiments performed by Ishihara and Nakaoka [13] and Ishihara [24]. The experimental setup is shown in Fig. 2. The size of the duct is 1420mm in length, 200 mm in height, and 234 mm in width. The duct is made of acrylic plates those have a thickness of 1 cm. The tube bank is set as shown in Fig. 2. The microphone is put on near the duct outlet as shown in Fig. 2. The flow is driven through the duct by a blower and the flow rate can be controlled by an inverter.

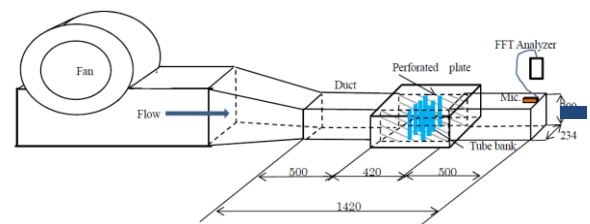


Figure 2. Experimental Setup.

The tube bank consists of an array of bronze tubes of diameter $D = 6$ mm. The array geometry is a square with spacing $T/D = 2.0$ and $L/D = 2.0$, where T is the transverse center-to-center spacing, L is the longitudinal center to center spacing and D is the tube outside diameter as shown in Fig. 3(a). The tube bank consists of 9 rows of tubes in the flow direction and 19 tubes in the direction perpendicular to the flow, and the length in the flow direction is 102 mm. The flow velocity in the duct is measured by using a hot wire anemometer and the sound pressure level of the self-sustained tone is measured using the microphone. An air is supplied to the duct by the blower and the air flow passes through the tube

bank. The vortex shedding occurs in and behind the tube bank. The vortex shedding frequency is proportional to the flow velocity. When it is close to the acoustic natural frequency of the duct system, then a high level sound occurs without a damping effect. The perforated plate is made of iron, and has a length of 400 mm, a height of 250 mm, and a thickness of 2.3mm. A hole with a diameter of 3 mm was opened in a staggered arrangement on a plate. As shown in Fig. 3(b), perforated plates can be mounted from the slit (shown in green), and the duct has two cavities with a depth of $L_c=100$ mm, 66 mm and 33 mm. A flow velocity measurement hole was provided at a position 125 mm upstream of the tube group, and the flow velocity was also measured there (U). The gap flow velocity is the flow velocity between the pipe and pipe, and the ratio of the area of the duct outlet to the area of the tube bank clearance is 1.95, hence the gap flow velocity V_g is obtained from the continuous equation, and results in $V_g = 1.95U$. The microphone was installed near the duct outlet shown in Fig. 2 using NL-20 manufactured by Rion. The C characteristic was used for measurement. Sound pressure signals are measured and converted to frequency domain with FFT Analyzer. The frequency range is from 100 Hz to 2000 Hz, the sampling frequency is 10000 Hz, the number of averages is 1000, and the frequency resolution is 20 Hz.

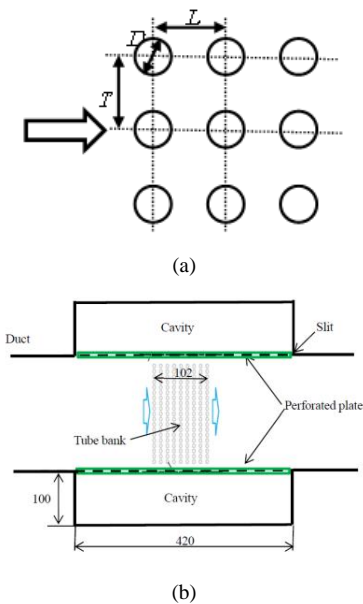


Figure 3. a) Array geometry of tube bank b) Detail of tube bank part with perforated plates.

B. Aperture Ratios of Perforated Plates

In this experiment, in order to examine the influence of the aperture ratio of the perforated plate on the self-sustained tone suppressing effect, as shown in Fig. 4, assuming a hole diameter of 3 mm, Ishihara and Nakaoka [13] made 6 patterns (1%, 2%, 4%, 8%, 16%, 32%) of the perforated plates. Here, the aperture ratio ϕ is the ratio of the area of the holes to the total area of the perforated plate and defined by Eq. (1).

$$\phi = \frac{n_h \left(\frac{\pi d^2}{4} \right)}{S_p} \quad (1)$$

Here, n_h is the number of the hole, $S_p=200 \text{ mm} \times 420 \text{ mm}$, is the total area of the perforated plate and d is the hole diameter (3 mm). Even at the same aperture ratio, if the hole diameter is different, the influence on self-sustained tone may be different. However in this study, it is assumed that the hole diameter is constant (3 mm) [13]. Since the case that the aperture ratio is 0% (holeless plate) is defined as the standard of this experiment, $\phi = 0\%$ is also a parameter of the aperture ratio.

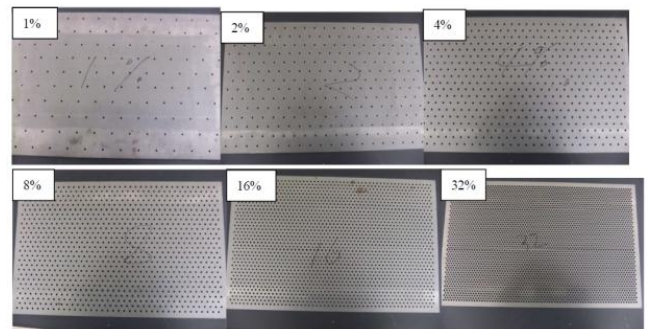


Figure 4. Perforated plates with several aperture ratios.

C. Experimental Results

Fig. 5 shows the sound pressure spectrum at each inverter frequency in the case of the aperture ratio $\phi = 0\%$. Inverter frequencies are 30, 40, 46 and 50 Hz, and corresponds to gap velocities 11.4, 15.7, 19.6 and 21.3 m/s, respectively. As shown in Fig. 5, the self-sustained tone slightly appears at $V_g = 19.6$ m/s, and clearly appears at $V_g = 21.3$ m/s. This peak frequency is 740 Hz. Fig. 6 shows the relation between overall sound pressure level and the gap velocity. The red line shows the case of the aperture ratio $\phi = 0\%$ (AR 0%), and the pale blue line shows the sound pressure level proportional to the 5th power law. The sound pressure level increases with increasing the gap velocity, and follows the 5th power law when the self-sustained tone is not generated (when the gap velocity is low). However, the sound pressure level suddenly increases when the self-sustained tone is generated (points surrounded by the blue circle). As shown in Fig. 6, the overall sound pressure level saturates, and remains high when the gap flow velocity is over 22m/s [13]. In this experiment, the self-sustained tone is generated when the gap velocity is over around 20 m/s. Therefore, if the Strouhal number St is 0.22, the vortex shedding frequency f_v is $f_v = St \cdot U/D = 0.22 \cdot 20/0.006 = 733 \text{ Hz}$. Meanwhile, the resonance frequency f_a in the duct width direction is $f_a = c/2L = 340/2/0.234 = 726.5 \text{ Hz}$. Considering the coupled mode in the longitudinal direction, the resonance frequency f_a is 736.3 Hz from Eq. (2), which is very close to the measured frequency of excitation at 740 Hz. Here, c is the sound speed (340 m/s), l_x and l_y are the duct width and the duct longitudinal length, respectively.

$$f_a = \frac{c}{2} \sqrt{\left(\frac{l}{l_x}\right)^2 + \left(\frac{m}{l_y}\right)^2} = \frac{340}{2} \sqrt{\left(\frac{1}{0.234}\right)^2 + \left(\frac{1}{1.42}\right)^2} = 736.6 \text{ Hz} \quad (2)$$

Fig. 6 also shows the measurement results of the relation between overall sound pressure level and the gap velocity in cases of aperture ratios $\phi = 1\%$, 2% , 4% , 8% , 16% and 32% . In general, duct noise follows the 5th to 8th power laws [24], and the noise generated in the duct in this experiment follows the 5th power law. Noise following the 5th power law is the ordinary aerodynamic noise. On the other hand, as shown by the blue circle in Fig. 6, the noise which does not follow the power law and becomes extremely large, is referred to as the self-sustained tone. As shown in Fig. 6, the self-sustained tone is generated only in the duct with the plate of the aperture ratio $\phi = 0\%$, which is the normal duct without holes. When the perforated plate with aperture ratios of $\phi = 1\%$ to 32% is applied on the duct wall surfaces, the overall sound pressure level rises along the 5th power law, and the self-sustained tone is not generated. Fig. 7 shows an effect of the aperture ratio on sound pressure level spectra at the gap velocity $V_g = 21.3 \text{ m/s}$. As shown in Fig. 7, the sound pressure decreases more than 30 dB in cases that the perforated plates and cavities are installed ($\phi \geq 0\%$), and the sound pressure level decreases in the high frequency region as the aperture ratio increases. Therefore, it is considered that the perforated plate has a sound absorbing property at high frequencies. However, as the aperture ratio increases, the flow rate flowing into holes of the perforated plate increase, especially when the aperture ratio is more than 8%. Consequently, the flow rate flowing into the tube bank decreases, and the generation of self-sustained tone and the practical cooling efficiency may be affected by the decrease of the flow rate into tube bank.

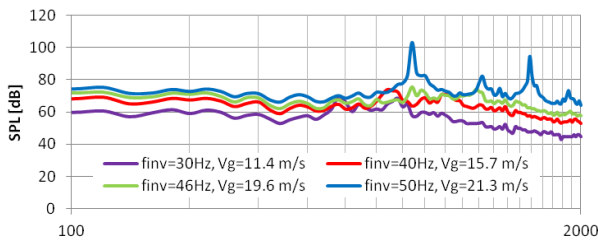


Figure 5. Spectra of sound pressure level in the case of aperture ratio $\phi=0\%$.

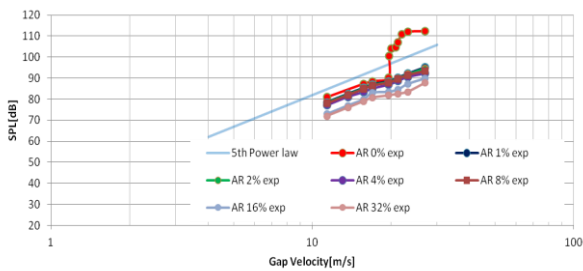


Figure 6. Relation between overall sound pressure level and the gap velocity in cases of aperture ratios ϕ (AR) = 0, 1, 2, 4, 8, 16 and 32%, and $L_c = 100 \text{ mm}$.

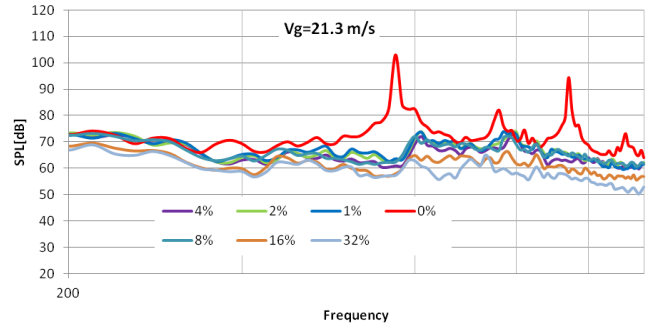


Figure 7. Relation between overall sound pressure level and the gap velocity in cases of aperture ratios $\phi = 0\%$, $\phi = 1\%$, 2% , 4% , 8% , 16% and 32% and $L_c = 100 \text{ mm}$.

Ishihara [24] studied experimentally the effect of a cavity volume which is used with perforated plates on the SPL. He concluded that the effect of a cavity volume on the SPL is a little. Figure 8 shows the effect of a cavity volume or depth on the sound pressure level in the case of the aperture ratio $\phi = 4\%$ as the typical example of the aperture ratio.

From the above, we perform the numerical simulations in the cases of the aperture ratios $\phi = 0\%$, $\phi = 1\%$, 2% and 4% , and depth of cavities $L_c = 100 \text{ mm}$.

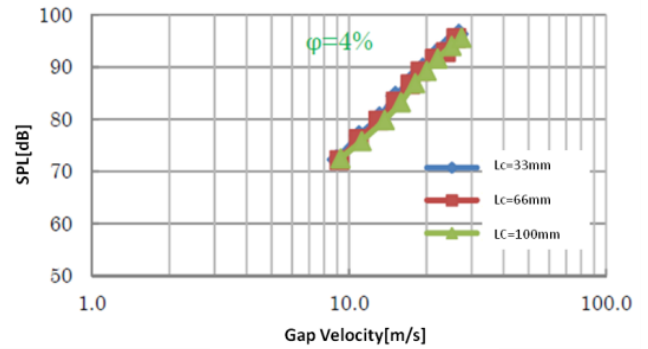


Figure 8. Relation between overall sound pressure level and the gap velocity in cases of aperture ratios $\phi = 4\%$ and $L_c = 100 \text{ mm}$, 66 mm and 33 mm .

III. NUMERICAL MODELLING

A. Transient CFD simulation

Unsteady flow fields in the duct are simulated in this paper. Inflow velocities are $U = 5.846, 7.026, 8.051, 8.564, 9.590, 10.923$ and 13.846 m/s , and corresponds to the gap velocities, $11.4, 13.7, 15.7, 16.7, 18.7, 21.3$ and 27.0 m/s , respectively. Reynolds numbers, Re_D , based on the gap velocity, V_g , is prescribed to be in the range of 4,600 to 10,800. Models for CFD simulations are shown in Fig. 9. For these simulations, a three-dimensional computational domain in the duct has been applied. Fig. 9(a) shows the computational domain for the normal duct without holes, which corresponds to the duct with the perforated plates of the aperture ratio $\phi = 0\%$. As an example of the computational domain with the perforated

plates, Fig. 9(b) shows the computational domain for the duct with the perforated plates of the aperture ratio $\phi = 2\%$. Fig. 9(c) shows a part of the computational domain near the perforated plates and cavities in the case of the aperture ratio $\phi = 2\%$. Unsteady flow fields are calculated using the commercial CFD code ANSYS Fluent version 17.0 using an implicit pressure-based coupled solver with second-order numerical accuracy in both space and time, and its compressible LES (Dynamic Smagorinsky model) calculation features. The origin of the Cartesian coordinate is placed at the center of the inflow boundary. The CFD domain contains 4,944,100 cells and 5,156,304 nodes for the case of the aperture ratio $\phi = 0\%$, 10,727,088 cells and 6,612,429 nodes for the case of the aperture ratio $\phi = 1\%$, 12,053,432 cells and 7,308,716 nodes for the case of the aperture ratio $\phi = 2\%$, and 13,646,420 cells and 8,004,142 nodes for the case of the aperture ratio $\phi = 4\%$, respectively. The cell spacing adjacent to the wall is 0.00025 m. In the wake region near the tube bank, the cell spacing is about 0.002 m. In the far wake region, the cell spacing is stretched to 0.006 m. A steady velocity and temperature (300 K) conditions are imposed on the inflow boundary. Zero pressure outflow and non-reflective boundary conditions are applied on the outflow boundary. No-slip and adiabatic conditions are applied on the other walls. Steady state simulations were performed using Spalart-Allmaras (S-A) turbulence model and then used as initial conditions of transient LES simulations. The unsteady simulations were performed for 10000 time steps with a time step size $dt = 1e-5s$, which corresponds to the non-dimensional time step based on f , 0.00733.

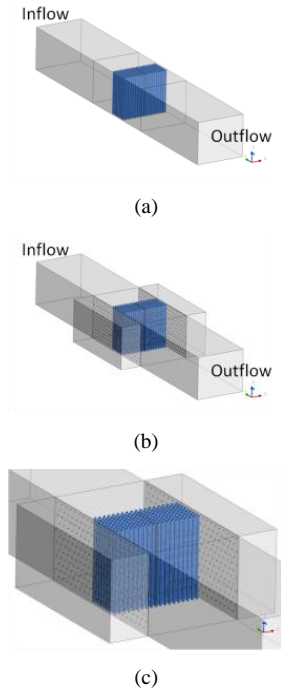


Figure 9. Computational domain for CFD simulation. (a) Normal duct without holes. (b) Duct with the perforated plates of the aperture ratio $\phi = 2\%$. (c) Duct near the perforated plates and cavities in the case of the aperture ratio $\phi = 2\%$.

B. Extraction of Acoustic Pressure on the duct wall in Frequency Domain

Generally, it is difficult to solve an aerodynamic noise radiation to a far field through a direct solution of a compressible Navier-Stokes equation, because it requires a high accuracy scheme in both space and time, a large computational domain which contains a noise source and propagation regions, a fine mesh enough to resolve a far field sound pressure fluctuation and a high computational cost [25]. Therefore, a hybrid approach in which the flow field (the noise source) and the acoustic propagation are solved separately, is generally used to calculate the aerodynamic noise radiation to the far field [26]. However, in this paper, the interaction between the flow and acoustic fields are need to be solved when the resonance or self-sustained tone occurs, a high level sound is generated and the monitor point is the noise source region. Therefore, the acoustic pressure is directly extracted from the unsteady compressible CFD simulations [27]. To convert the acoustic pressure time histories obtained from CFD simulations into the frequency spectra, the discrete Fourier transform (DFT) has been applied. The acoustic pressure are extracted from 2500 steps (from $t = 0.05$ s to 0.1 s). The sampling period is $2e-5$ s.

C. Acoustic Simulation

The BEM solver in commercial acoustic simulation package, WAON, is used to solve the acoustic characteristics [26]. In a sound field that satisfies the three dimensional Helmholtz equation, the Kirchhoff-Helmholtz integral equation [28] for sound pressure is described as follows with respect to a point i and an area S of a surface on a boundary. In this solver, the following simultaneous linear equation is solved:

$$\frac{1}{2}P(\mathbf{r}_i) = \int_{\Gamma} \left(P(\mathbf{r}_q) \frac{\partial G(\mathbf{r}_i, \mathbf{r}_q)}{\partial n_q} - \frac{\partial P(\mathbf{r}_q)}{\partial n_q} \right) dS + p_d(\mathbf{r}_q) \quad (3)$$

In this solver, the following simultaneous linear equation is solved:

$$(\mathbf{E} + \mathbf{B} + \mathbf{C})\mathbf{p} = j\omega\rho\mathbf{A} + \mathbf{p}_d \quad (4)$$

Here, \mathbf{p} is the acoustic pressure vector, \mathbf{v} is the particle velocity vector and the entries of the influence coefficient matrices are represented as follows:

$$E_{ij} = \frac{1}{2} \delta_{ij}, \quad (5)$$

$$A_{ij} = \int_{\Gamma_j} N_j(\mathbf{r}_q) G(\mathbf{r}_i, \mathbf{r}_q) dS_q, \quad (6)$$

$$B_{ij} = \int_{\Gamma} N_j(\mathbf{r}_q) \frac{\partial G(\mathbf{r}_i, \mathbf{r}_q)}{\partial n_q} dS_q, \quad (7)$$

$$C_{ij} = \frac{jk}{z_j} \int_{\Gamma_2} N_j(\mathbf{r}_q) G(\mathbf{r}_i, \mathbf{r}_q) dS_q, \quad (8)$$

$$G(\mathbf{r}_i, \mathbf{r}_q) = \frac{e^{jk|\mathbf{r}_p - \mathbf{r}_s|}}{4\pi|\mathbf{r}_p - \mathbf{r}_s|} \quad (9)$$

where δ_{ij} is Kronecker's delta, and Γ_v is a vibration boundary and a part of Γ . Γ_a is an absorption boundary and a part of Γ . \mathbf{r}_i is the position vector at the node i , \mathbf{r}_q is the position vector of the source point q and N_j is the interpolation function of the node j . z_j is the acoustic impedance

ratio at the node j . G is the fundamental solution of a three dimensional sound field. With the number of nodes N , the component p of the vector \mathbf{p} is expressed as follows:

$$p(\mathbf{r}_q) = \sum_{j=1}^N N_j(\mathbf{r}_q)p_j \quad (10)$$

The component p_d of the vector \mathbf{p}_d is the direct pressure contribution from the acoustic source, and expressed as follows:

$$p_d(\mathbf{r}_p) = -j\omega\rho QG(\mathbf{r}_i, \mathbf{r}_q) \quad (11)$$

where ρ is the density kg/m³ and Q is the volume velocity m³/s. \mathbf{r}_p is a position vector of the monitor point. Fig. 10 shows boundary element models. Fig. 10(a) shows the boundary element model for the case of the aperture ratio $\phi = 0\%$, and Fig. 10(b) shows a part of the boundary element model near the perforated plates and cavities in the case of the aperture ratio $\phi = 2\%$.

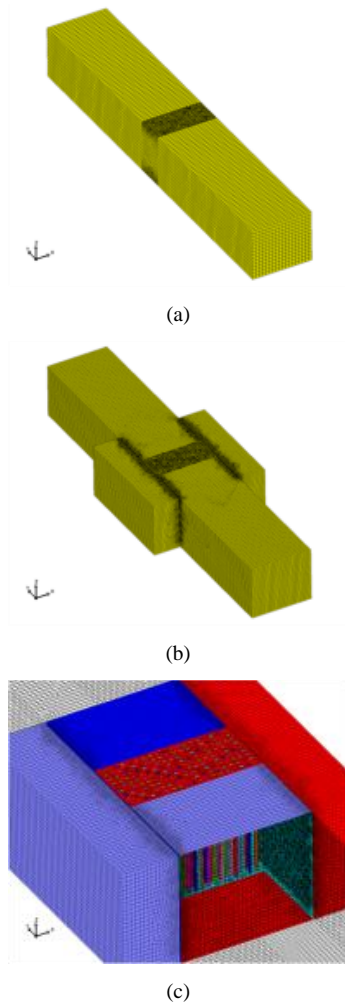


Figure 10. Boundary element model. (a) Aperture ratio $\phi = 0\%$. (b) Aperture ratios $\phi = 1\%$, 2% , and 4% . (c) Near the perforated plates and cavities in the case of the aperture ratio $\phi = 2\%$.

There are 80,530 boundary elements for the case of the aperture ratio $\phi = 0\%$, 167,361 boundary elements for the case of the aperture ratio $\phi = 1\%$, 226,079 boundary elements for the case of the aperture ratio $\phi = 2\%$ and 307,747 boundary elements for the case of the aperture ratio $\phi = 4\%$, respectively. The maximum element size is 0.013 m. To concern acoustic waves moving from the inflow boundary to the outside, an impedance boundary condition is imposed at the inflow boundary, whose value is ρc . The outflow boundary is the surface connecting the duct inside and outside. At the outflow boundary, the interface boundary, where the particle velocity and acoustic pressure of the internal and external sound fields of the duct are coupled, is imposed. At other wall boundaries except the holes, weak absorption boundaries, whose absorption coefficient is 0.02, is imposed. The absorption coefficient “0.02” corresponds to that of the general acrylic surface. To clarify the acoustic characteristics of the tube bank duct, the acoustic frequency responses have been calculated using the monopole point sources (without the flow) shown in Fig. 11. The magnitude of the point sources is 1 Pa in all frequencies. The point source is located at $(0.25H, -3.86H, 0)$ downstream side of the tube bank, where H is 200 mm in the height of the tube bank duct. In the self-sustained tone phenomenon with the flow, the sound source is supposed to be vortices generated on the downstream side behind the tube. Therefore, the sound source was placed on the downstream side of the tube bank also in the acoustic simulations. Furthermore, in order to excite the resonance mode in the duct width direction, the sound source was arranged asymmetrically with respect to the YZ plane.

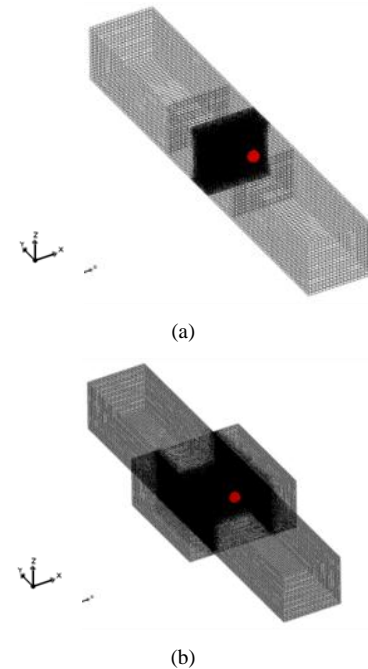


Figure 11. Position of monopole point source. (a) Aperture ratio $\phi = 0\%$. (b) Aperture ratios $\phi = 1\%$, 2% , and 4%

IV. RESULTS AND DISCUSSIONS

A. CFD Simulation Results (Aperture Ratio $\phi = 0\%$)

Instantaneous snapshots of velocity and vorticity fields at $Z = 0$ plane are shown in Figs. 12(a), (b), (c) and (d), for the cases of $V_g = 21.3$ m/s and $V_g = 11.4$ m/s. Vortices generated around tubes travels downstream and form a vortex street. In the case of $V_g = 21.3$ m/s, vortices are stronger than in the case of $V_g = 11.4$ m/s. Figs. 12(e) and (f) show instantaneous snapshots of fluctuation pressure field at $Z = 0$ plane, which is defined as follows [15].

$$dp = p_s - p_{mean} \quad (12)$$

Here, p_s is the static pressure which is defined by $p_s = p - p_0$ and p_{mean} is the time-averaged of the pressure. The symbol p_0 denotes the ambient pressure. Comparing the cases of $V_g = 27.0$ m/s with $V_g = 11.4$ m/s, the fluctuation pressure in the case of $V_g = 21.3$ m/s is much larger than in the case of $V_g = 11.4$ m/s. In the case of $V_g = 21.3$ m/s, the pressure fluctuation mode in the width direction of the duct clearly appears.

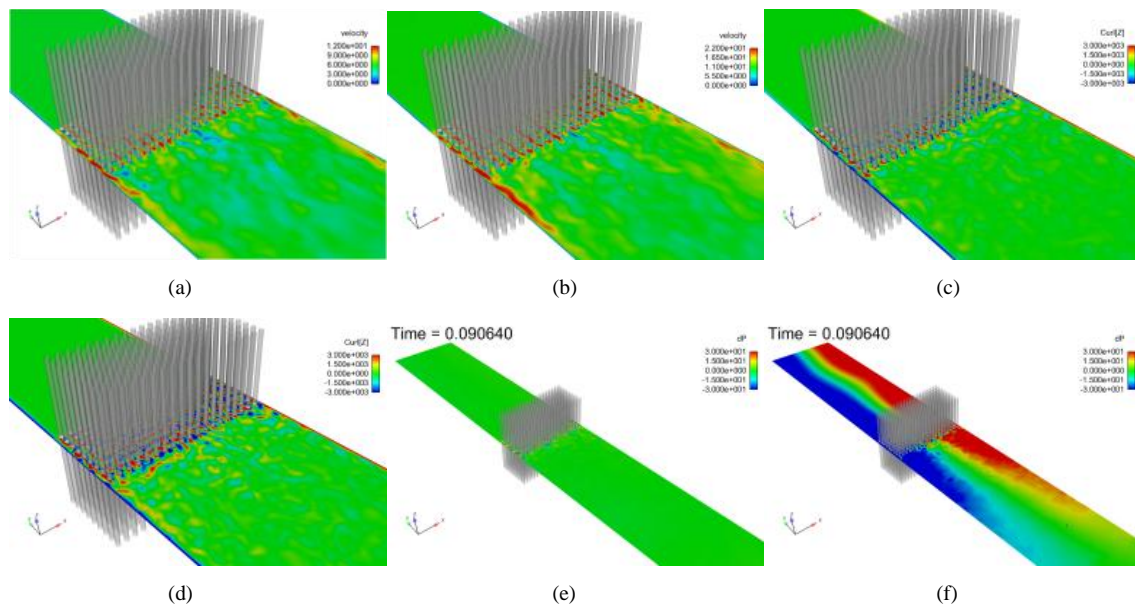


Figure 12. Velocity, vorticity and fluctuation pressure fields in the case of aperture ratio $\phi = 0\%$. (a) Velocity at $V_g = 11.4$ m/s, (b) Velocity at $V_g = 21.3$ m/s. (c) Vorticity at $V_g = 11.4$ m/s, (d) Vorticity at $V_g = 21.3$ m/s. (e) Fluctuation Pressure at $V_g = 11.4$ m/s, (f) Fluctuation Pressure at $V_g = 21.3$ m/s.

Fig. 13 shows the frequency spectra of SPL on the wall of the duct near the outflow boundary. Both the simulated and measured data are shown in Fig. 13. In both simulations and experiments, the self-sustained tone occurs in the case of $V_g = 21.3$ m/s, and the self-sustained tone does not occur in the case of $V_g = 11.4$ m/s. In the case of $V_g = 21.3$ m/s, the peak of self-sustained tone appears at about 740 Hz and its high harmonic frequency, 1480 Hz. This frequency 740 Hz is close to the resonance frequency in the duct width direction, 726.5 Hz and that in the coupled mode in the longitudinal direction, 736.3 Hz, as mentioned in II-C. It can be presumed that the slight difference in the resonance frequencies obtained from the theory (without the flow) and the CFD simulation or the experiments is due to the absence or presence of the flow. This is because the resonance frequency slightly increases with increasing the gap flow velocity, as shown in the Fig. 1 [15]. The predicted SPL of the dominant tone at 740 Hz reasonably agrees with the measured one. The generation of the higher harmonic at 1480 Hz, which is surrounded by the red circle in Fig. 13, is also predicted as in the experiments. However, the SPL of the higher harmonic is slightly lower than the experiments. Besides, there are some peaks between 900 Hz

and 1050 Hz in the CFD results, and those are larger than the experiments. These could probably be due to the mesh size, number of the mesh, time step and time duration used in the CFD simulations. However, the predicted SPL of the dominant tone, that is assumed to contribute most to the overall SPL when the self-sustained tone occurs, reasonably agrees with the measured one. Therefore, in this paper, we applied the mesh size and time step size to the other cases, and perform the CFD simulations.

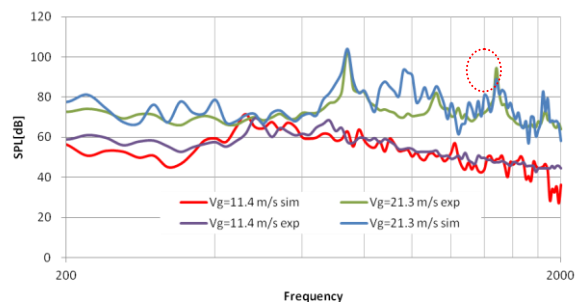


Figure 13. Spectra of sound pressure level in the case of aperture ratio $\phi = 0\%$.

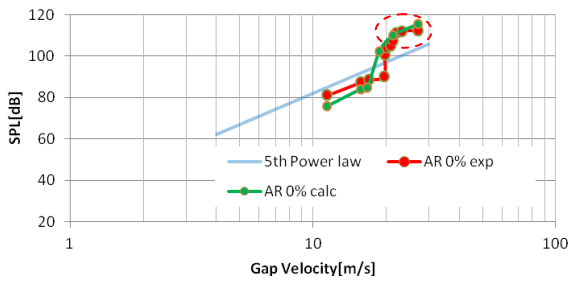


Figure 14. Relation between overall sound pressure level (200-2000Hz) and gap velocity in the case of aperture ratio $\phi = 0\%$ (AR 0%).

Fig. 14 shows the relation between overall sound pressure level and the gap velocity in both simulations and experiments. In the simulations as well as the experiments, the sound pressure level increases with increasing the gap velocity and follows the 5th power law when the gap velocity is low. However, the sound pressure level does not follow the 5th power law when the gap velocity is high (points surrounded by the red circle), and remains high with increasing the gap velocity. As shown in Figs. 13 and 14, the simulations show a reasonable agreement with the experiments in terms of the generation prediction of the self-sustained tone. Fig. 15 shows the SPL on the wall of the duct at 740 Hz. The SPL fields are obtained from the CFD simulations using DFT. In CFD simulations, as shown in Fig. 15, the acoustic mode does not clearly appear in the case of $V_g = 11.4$ m/s, however, that clearly appears in the case of $V_g = 21.3$ m/s, as in the experiments. Fig. 15(b) shows that the acoustic mode in the width direction or the coupled mode in the width and longitudinal directions appears at 740 Hz in the case of $V_g = 21.3$ m/s. The acoustic mode at 740 Hz shown in Fig. 15(b) corresponds to the fluctuation pressure field in Fig. 12(f). Accordingly, the acoustic mode in the duct width direction or the coupled mode in the duct width and longitudinal directions is dominant in the self-sustained tone. This mode is close to the acoustic mode obtained from the Eq. (2) and the experiments.

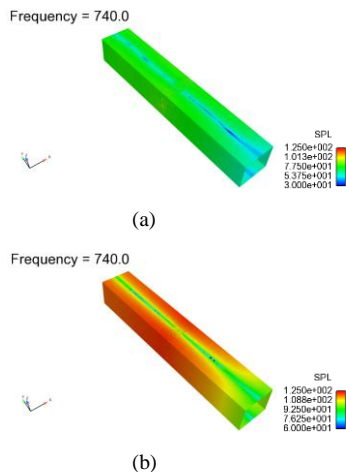


Figure 15. SPL on the wall of the duct in the case of aperture ratio $\phi = 0\%$. (a) $V_g = 11.4$ m/s. (b) $V_g = 21.3$ m/s.

B. CFD Simulation Results (Aperture Ratio $\phi = 1, 2,$ and 4%)

Instantaneous snapshots of velocity field at $V_g = 21.3$ m/s are shown in Fig. 16. Fig. 16 shows that velocity distributions in the duct are similar in all cases of the aperture ratios. Regardless of the aperture ratio, the flow is flowing into the tube bank at almost the same velocity in all cases of the aperture ratios.

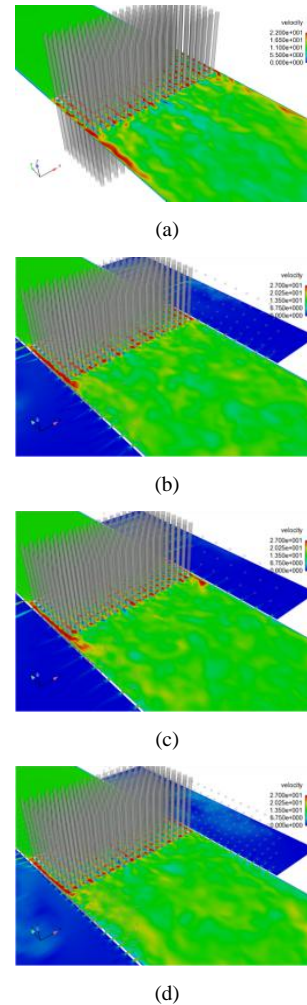


Figure 16. Velocity fields in the cases of aperture ratio $\phi = 0, 1, 2$ and 4% at $V_g = 21.3$ m/s. (a) $\phi = 0\%$ at $z = 0$ m plane. (b) $\phi = 1\%$ at $z = 0.11$ m plane. (c) $\phi = 2\%$ at $z = 0.112$ m plane. (d) $\phi = 4\%$ at $z = 0.107$ m plane.

With the perforated plates, a part of the flow passes through the holes of the perforated plates, and the flow rate flowing into the tube bank decreases. To clarify the rate of flow into perforated plates, the leak ratio was defined and examined. The flow leak ratio (LR) is defined as follows.

$$LR = \frac{Q_{p1} + Q_{p2}}{Q_{out}} \quad (13)$$

Here, as shown in Fig. 17(a), Q_{p1} and Q_{p2} are the time-averaged flow rate (m³/s) flowing into holes of the perforated plates on the upstream side, and Q_{out} is the time-averaged flow

rate on the downstream side. Fig. 17(b) shows the relation between flow leak ratio and aperture ratio. As shown in Fig. 16, the flow leak ratio is below the 6.6% at all aperture ratio, and the effect of the flow leak on the generation of self-sustained tone and the practical cooling efficiency seems to be small.

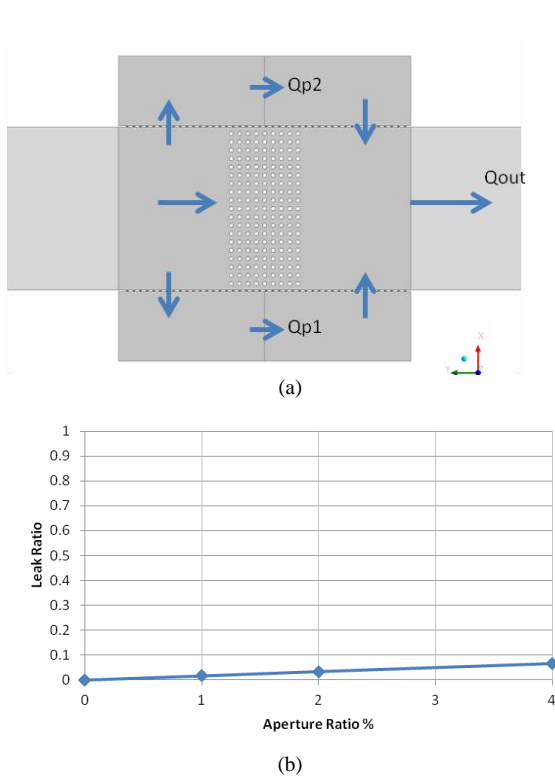


Figure 17. Relation between flow leak ratio and aperture ratio.

Fig. 18 shows instantaneous snapshots of the fluctuation pressure field. Comparing the cases of $\phi = 0\%$ with $\phi = 1, 2$ and 4% , the fluctuation pressure in the case of $\phi = 0\%$ is much larger than that in the cases of $\phi = 1, 2$ and 4% . In the cases of $\phi = 1, 2$ and 4% , the pressure fluctuation mode in the duct width direction does not appear.

Fig. 19 shows the effect of the aperture ratio on the frequency spectra of SPL on the wall of the duct near the outflow boundary. For comparison, both the simulated and measured data are shown, and the frequency spectra of SPL in the case of $\phi = 0\%$ is also displayed in Fig. 19. In both simulations and experiments, the self-sustained tone occurs in the case of $\phi = 0\%$, however the self-sustained tone does not occur in the cases of $\phi = 1\%$.

Fig. 20 shows the effect of the aperture ratio on the overall sound pressure level. The SPL decreases with increasing the aperture ratio, and rapidly decreases when the aperture ratio is

between 0 and 1%. The measurement and simulation data are in reasonable agreement in terms of prediction of the effect of perforated plates on the self-sustained tone, as shown in Fig. 20.

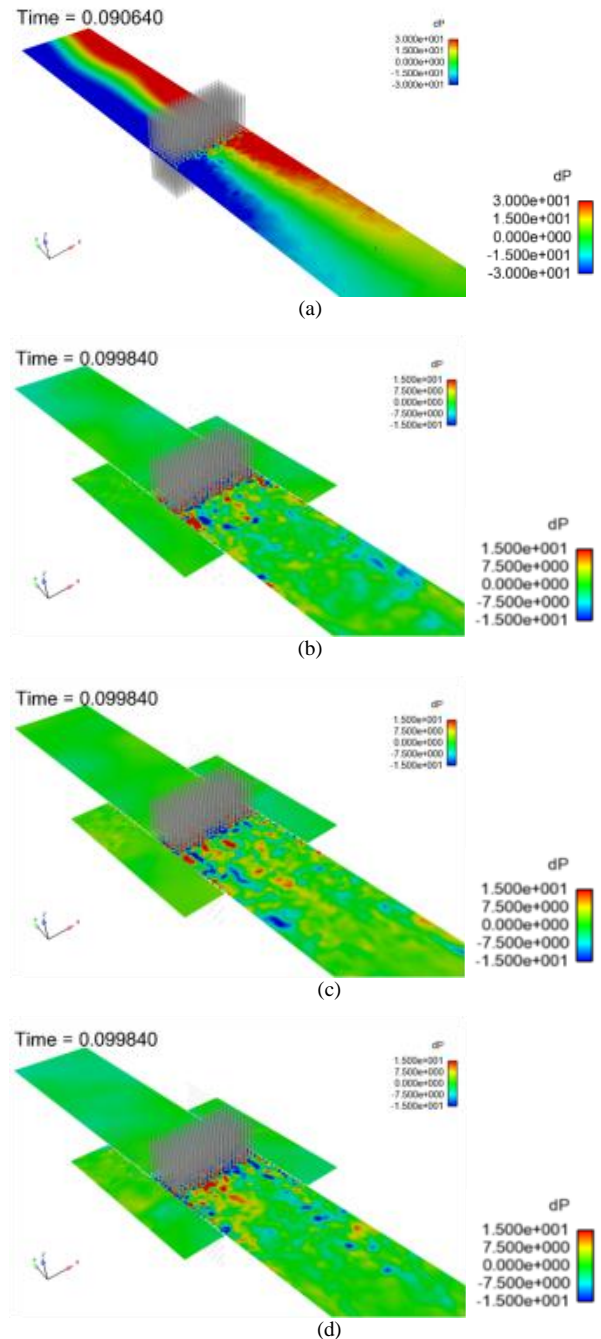


Figure 18. Fluctuation pressure fields in the cases of aperture ratio $\phi = 0, 1, 2$ and 4% at $V_g = 21.3$ m/s. (a) $\phi = 0\%$ at $z = 0$ m plane. (b) $\phi = 1\%$ at $z = 0.01$ m plane. (c) $\phi = 2\%$ at $z = 0.012$ m plane. (d) $\phi = 4\%$ at $z = 0.007$ m plane.

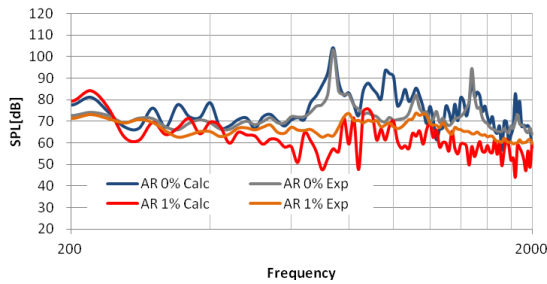


Figure 19. Effect of aperture ratio on frequency spectra of SPL at $V_g = 21.3$ m/s. $\phi = 1\%$.

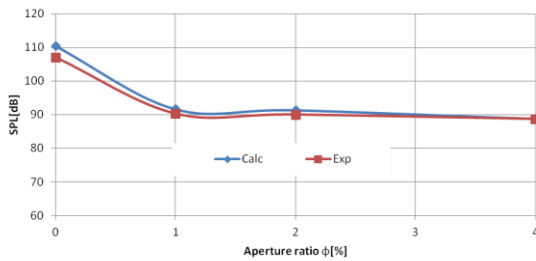


Figure 20. Effect of aperture ratio on overall sound pressure level (200-2000Hz) at $V_g = 21.3$ m/s.

Fig. 21 shows the SPL on the wall of the duct in frequency domain at the peak frequency, 740 Hz. In the case of $\phi = 0\%$, the acoustic mode clearly appears as shown in Fig. 21(a). On the other hand, in the cases of $\phi = 1\%$, the acoustic mode does not clearly appear and the value of SPL on the duct wall is close to 40 dB smaller than that in the case of $\phi = 0\%$, as shown in Fig. 21(b).

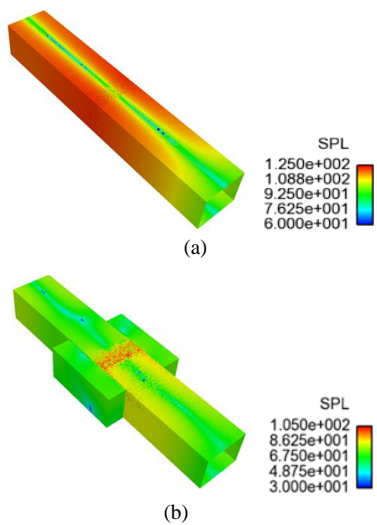


Figure 21. SPL on the wall of the duct at $V_g = 21.3$ m/s. (a) $\phi = 0\%$. (b) $\phi = 1\%$

Fig. 22 shows the relation between overall sound pressure level and the gap velocity in the cases of $\phi = 0\%$ and 1% . As shown in Fig. 22, the self-sustained tone is generated in the case of $\phi = 0\%$, and the sound pressure level does not follow the 5th power law when the gap velocity is high, as mentioned in IV-A. However, in the case of $\phi = 1\%$, the self-sustained tone is not generated, and regardless of the gap velocity, the overall sound pressure level rises along the 5th power law in both simulations and experiments. Therefore, when the perforated plate is applied on the duct wall surfaces, the self-sustained tone does not occur in the CFD simulations, as in the experiments [13].

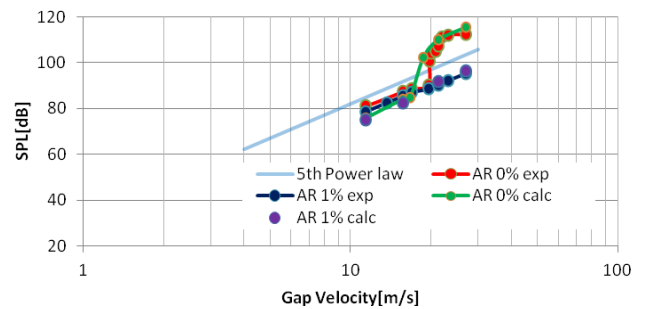


Figure 22. Relation between overall sound pressure level (200-2000Hz) and gap velocity in cases of aperture ratios $\phi = 0\%$ and $\phi = 1\%$.

C. Acoustic Simulation Results

To clarify acoustic characteristics of the tube bank duct with perforated plates, the acoustic frequency responses have been calculated using the monopole point source (without the flow) shown in Fig. 11. The monitor point is located at $(0.585H, -4.76H, 0)$ downstream side of the tube bank. Figs. 23(a) and (b) show the spectra from 100 to 2000 Hz, and the spectra from 700 to 1000 Hz, respectively. In the case of $\phi = 0\%$, the peak frequency surrounded by the green circle is 725 Hz, and close to the resonance frequency in the duct width direction, as mentioned in III-C. The peak frequency surrounded by the black circle is 1440 Hz, and is close to a higher harmonics of the resonance frequency in the duct width direction. On the other hand, in the cases of $\phi = 1, 2$ and 4% , peak frequencies surrounded by blue, red and purple circles are close to the resonance frequency in the duct width direction, and change to higher frequencies than that in the case of $\phi = 0\%$ with increasing the aperture ratio.

Table.1 shows the peak frequency in each case of the aperture ratio. It has been also confirmed that the resonance frequency increases as the aperture ratio increases in our previous study [29], in which an acoustic resonance frequency has been experimentally and analytically verified by assuming a one-dimensional sound field in a duct partitioned by a perforated plate, and similar results are obtained in this study.

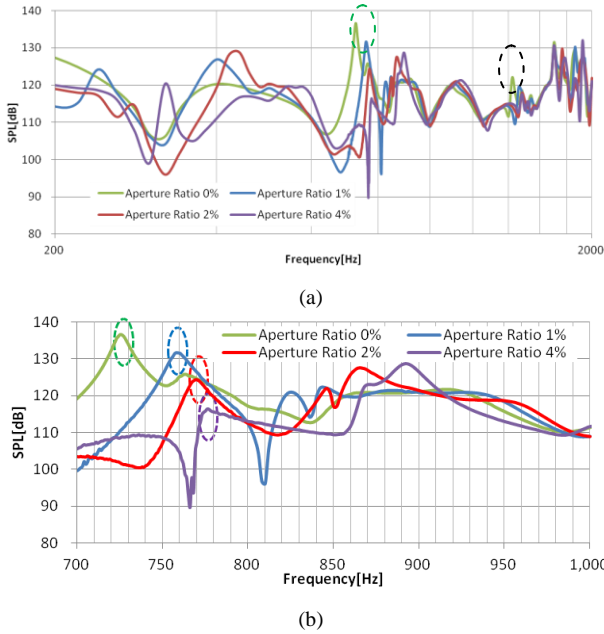


Figure 23. Acoustic frequency responses. (a) Spectra from 100 to 2000 Hz. (b) Spectra from 700 to 1000 Hz.

TABLE I. PEAK FREQUENCY IN EACH CASE OF THE APERTURE RATIO.

Method, Aperture Ratio	Resonance Frequency
Theory (Aperture Ratio 0 %, without flow)	726.5 Hz
BEM (Aperture Ratio 0 % without flow)	725 Hz
BEM (Aperture Ratio 1 % without flow)	758 Hz
BEM (Aperture Ratio 2 % without flow)	769 Hz
BEM (Aperture Ratio 4 % without flow)	774 Hz

To investigate the effect of the aperture ratio of the perforated plates on the resonance frequency in the duct width direction mode, we investigated the acoustic pressure profile from the center of the duct to the cavity. Fig. 24 shows profile lines and acoustic pressure profile in each case of the aperture ratio. The sound pressure profiles at the resonance frequency in the duct width direction mode are shown in Fig. 24(e). As shown in Fig. 24(e), the sound pressure suddenly decreases near the hole by the sound pressure passing through the holes. Black points in Fig. 24(e) are the points where the sound pressure is at its maximum value. In the case of $\phi = 0\%$ (without the perforated plates), the position where the sound pressure in the resonance frequency in the duct width direction mode is at its maximum value, is on the side wall of the duct. However, in the cases of $\phi = 1, 2$ and 4% (with the perforated plates), the position where the sound pressure is at its maximum value shifts slightly from the side wall to the center of the duct.

Table.2 shows the 1/4 wave length, wave length and resonance frequency calculated from the 1/4 wave length. The

1/4 wave length is estimated from the distance from the center of the duct to the position where the sound pressure is at its maximum value in Fig. 24(e). The resonance frequency calculated from the 1/4 wave length in each case of the aperture ratio in Table.2 is close to that calculated from the acoustic simulations in Table.1. It seems that the sound pressure easily escapes through the holes of the perforated plates to cavities as the aperture ratio and number of the holes increase. As a result, the region where the sound pressure decreases near the side wall of the duct, increases and the position where the sound pressure in the duct width direction mode is at its maximum value shifts from the side wall to the center of the duct as the aperture ratio increases. Fig. 25 shows the acoustic mode at each peak frequency in the cases of $\phi = 0, 1, 2$ and 4% . In the case of $\phi = 0\%$, the acoustic mode in the width direction strongly appears at 725 Hz. However, in the cases of $\phi = 1, 2$ and 4% , the acoustic mode in the duct width direction does not clearly appear, and the value of SPL decreases as the aperture ratio increases. From the point of view of the acoustic energy, Fig. 26 shows the contour and vector of the acoustic intensity level on inflow, outflow boundaries, z plane around the tube bank, and cross sections in the holes between the cavities and duct for the cases of $\phi = 0$ and 4% at each of the peak frequency. The length of the vector shown in Figs. 26 (c) and (d) corresponds to the strength of the acoustic intensity level and the direction of the vector corresponds to that of the acoustic energy flow. In the case of $\phi = 0\%$, the acoustic energy generated in the duct, is released only to the outside of the duct from inflow and outflow boundaries, as shown in Figs. 26(a) and (c). However, in the case of $\phi = 4\%$, the acoustic energy is released to the cavities through the holes of the perforated plates as well as the outside of the duct, and the acoustic intensity level on the inflow and outflow boundaries is much lower than that in the case of $\phi = 0\%$ as shown in Figs. 26(b) and (d). It indicates that a part of the acoustic energy is released to the cavities through the holes, and as a result, the acoustic energy released to the outside is reduced.

As above, it was found that the sound pressure level near the resonance frequency in the duct width direction is attenuated when the perforated plate is applied on the duct wall surfaces. From the frequency responses in Fig. 23(b), the acoustic damping ratio was calculated by the half-power band width method. The acoustic damping ratio is expressed by the following equation.

$$\zeta = \frac{\Delta f}{2f_n} \quad (14)$$

Here, f_n is the resonance frequency in the width direction of the duct, and Δf is the difference $|f_1 - f_2|$. f_1 and f_2 are the frequencies at points 3 dB lower than the peak value of the sound pressure level. Fig. 27 shows the effect of the aperture ratio on the acoustic damping. In the cases of $\phi = 1, 2$ and 4% , the acoustic damping ratio is larger than that in the case of $\phi = 0\%$. Therefore, it was also numerically confirmed that the perforated plate has an effect of attenuating sound.

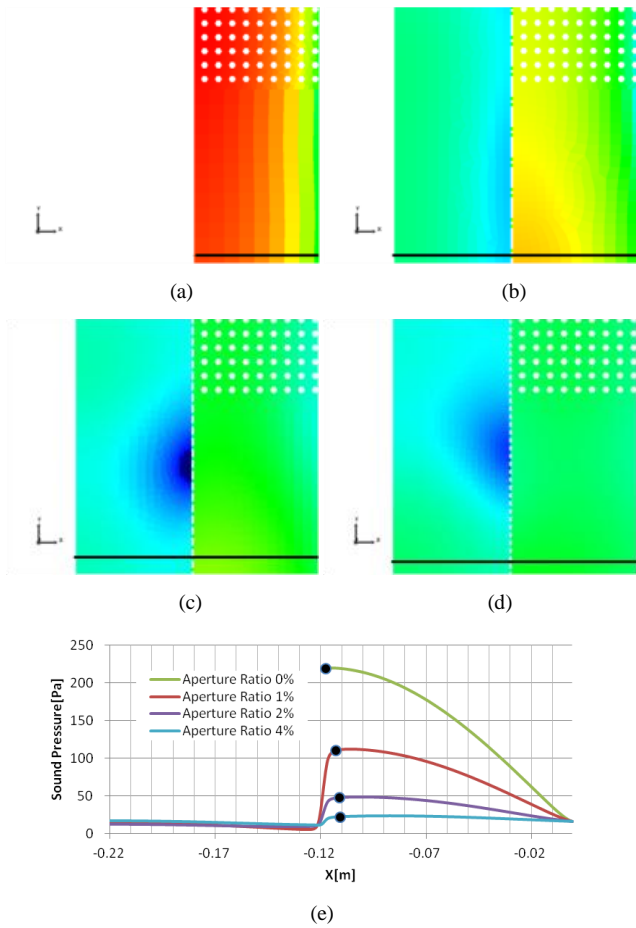


Figure 24. Acoustic pressure profile in the resonance frequency in the duct width direction mode on the line from the center of the duct to the cavity in each case of the aperture ratio. Profile lines (a) in the case of $\phi = 0$ at $z = 0$ m plane, (b) in the case of $\phi = 1$ at $z = 0.01$ m plane, (c) in the case of $\phi = 2$ at $z = 0.012$ m plane, and (d) in the case of $\phi = 4$ at $z = 0.007$ m plane. (e) Acoustic pressure profile and peak point in each case of the aperture ratio

TABLE II. PEAK FREQUENCY IN EACH CASE OF THE APERTURE RATIO.

Method, Aperture Ratio	1/4 Wave length	Wave length	Frequency
BEM (Aperture Ratio 0 % without flow)	0.117 m	0.468	726.49 Hz
BEM (Aperture Ratio 1 % without flow)	0.112 m	0.448	758.92 Hz
BEM (Aperture Ratio 2 % without flow)	0.111 m	0.444	765.77 Hz
BEM (Aperture Ratio 4 % without flow)	0.110 m	0.440	772.72 Hz

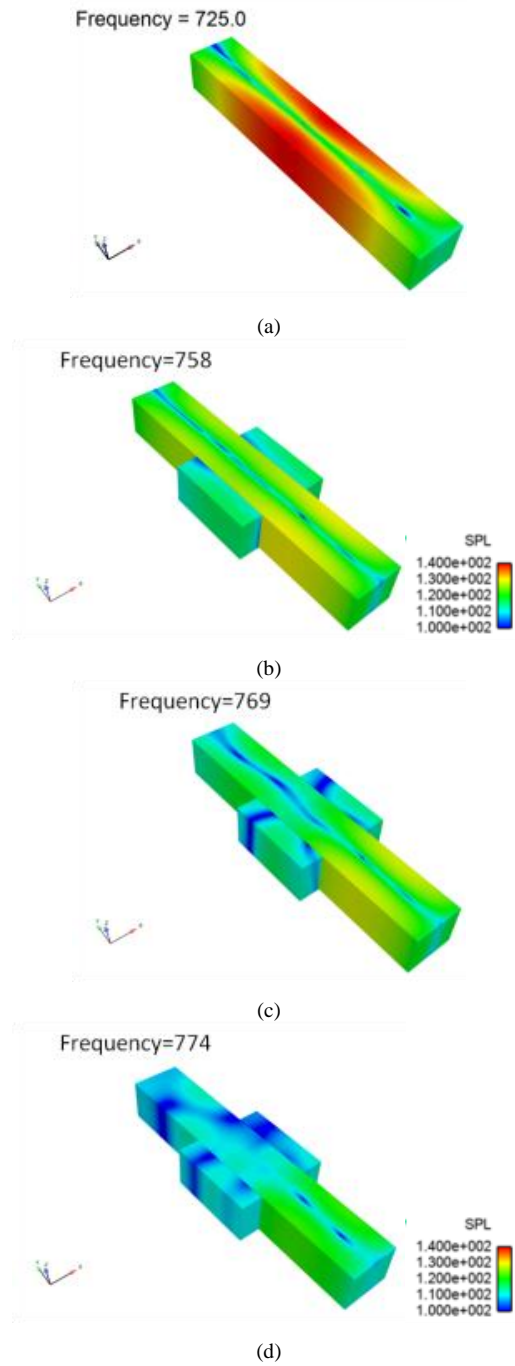


Figure 25. Acoustic modes at each peak frequency in the cases of $\phi = 0, 1, 2$ and 4%. (a) $\phi = 0\%$. (b) $\phi = 1\%$. (c) $\phi = 2\%$. (d) $\phi = 4\%$.

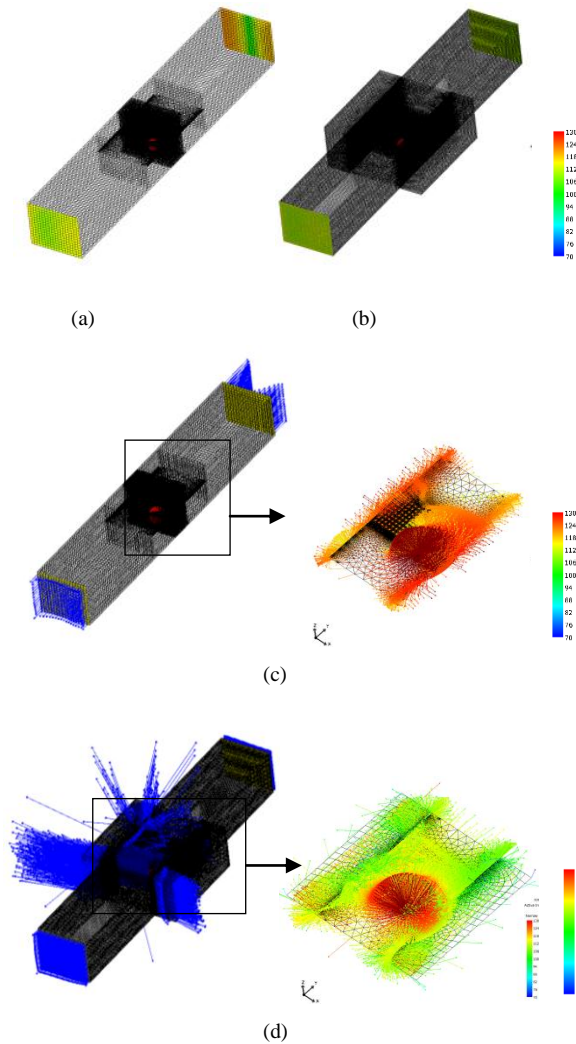


Figure 26. Acoustic intensity level on inflow, outflow boundaries, z plane around the tube bank and cross sections in the holes. (a) Contour, $\phi = 0\%$ at 740 Hz. (b) Contour, $\phi = 4\%$ at 774 Hz. (c) Vector, $\phi = 0\%$ at 740 Hz. (d) Vector, $\phi = 4\%$ at 774 Hz.

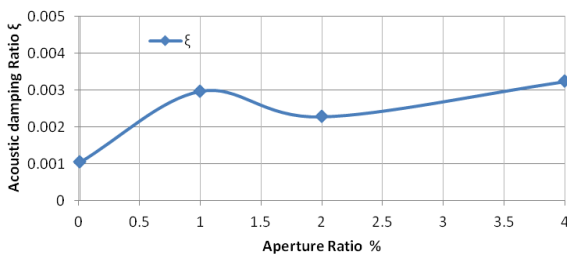


Figure 27. Effect of aperture ratio on acoustic damping.

V. CONCLUSION

In this paper, to verify the effect of the aperture ratio of the perforated plate on the self-sustained tone and acoustic resonance frequencies numerically, we have performed

compressible CFD and acoustic simulations, and compared the simulation results with the measurements. The following concluding remarks are obtained in this paper.

- In CFD simulations, the self-sustained tone is suppressed in all cases of the aperture ratio $\phi \Rightarrow 0.01$ (1%) of the perforated plates applied on the duct wall as in the experiments. The measurement and simulation data are in reasonable agreement in terms of prediction of the effect of perforated plates on the self-sustained tone.
- The self-sustained tone is generated in the case of $\phi = 0\%$ (when the perforated plates are not applied on the duct wall), and the sound pressure level does not follow the 5th power law when the gap velocity is high. However, in the case of $\phi = 1\%$ (when the perforated plates are applied on the duct wall), the self-sustained tone is not generated, and regardless of the gap velocity, the overall sound pressure level rises along the 5th power law in both simulations and experiments.
- In acoustic simulations without the flow, it was found that the resonance frequency in the duct width direction increases when the perforated plates are applied on the duct wall and the perforated plate has a sound absorption effect. The acoustic energy is released to the cavities through the holes of the perforated plates as well as the outside of the duct when the perforated plates and cavities are applied on the duct wall. As a result, the acoustic energy released to the outside of the duct is much lower and the acoustic damping ratio is larger than when the perforated plates are not applied on the duct wall. Consequently, it is considered that the self-sustained tone is suppressed by increasing the resonant frequency in the duct width direction and sound absorbing effect of the perforated plate, when the perforated plates are applied on the duct wall.

REFERENCES

- [1] R. C. Baird, Pulsation-induced vibration in utility steam generation unit, *Combustion*, 25, 1954, p.38-44.
- [2] P. R. Owen, Buffeting excitation of boiler tube vibration, *Journal of Mechanical Engineering Science*, (4), 1965, p.431-439.
- [3] Y. N. Chen, Flow-induced vibration and noise in tube-bank heat exchangers due to von karman streets, *Journal of Engineering for Industry*, 90 (1), 1968, p.134-146.
- [4] M. Fnunakawa, R. Umakoshi, The acoustic resonance in a tube bank, *Bulletin of JSME*, 13 (57), 1970, p.348-355.
- [5] J. A. Fitzpatric, The prediction of flow-induced noise in heat exchanger tube arrays, *Journal of Sound and Vibration*, 99 (3), 1985, p.425-435.
- [6] R. D. Blevins, M. M. Bresser, Acoustic resonance in heat exchanger tube bundles-part 1: Physical nature of the phenomena, *Journal of Pressure Vessel Technology*, 109 (3).
- [7] D. S. Weaver, Vortex shedding and acoustic resonance in heat exchanger tube arrays, *Technology for the 90's*, ASME Special Publication, New York, 1993, p.776-810.
- [8] H. Hamakawa, H. Matsue, E. Nishida, T. Fukano, Acoustic resonance and vortex shedding from tube banks of boiler plant, *Journal of Fluid Science and Technology*, 3 (6), 2008, p.805-813.
- [9] R. Hanson, S. Ziada, Effect of acoustic resonance on the dynamic lift of tube arrays, *Journal of Fluids and Structures*, 27 (3), 2011, p.367-382.

- [10] S. Ziada, A. Oregören, Vortex shedding in an in-line tube bundle with large tube spacings, *Journal of Fluids and Structures*, 7 (6), 1993, p.661-687.
- [11] H. Hamakawa, H. Matsue, E. Nishida, T. Fukano, Effect of arrangement of tube banks on acoustic resonance, *Open Journal of Fluid Dynamics*, 2 (4A), 2012, p.311-317.
- [12] K. Ishihara, T. Tamehira, M. Tsujii, M. Ichimiya, Study on a countermeasure of self-sustained tone by a baffle plate in boiler tube banks, *Journal of Basic and Applied Physics*, 2 (3), 2013, p.148-154.
- [13] K. Ishihara, M. Nakaoka, Study on a countermeasure using walls made of perforated plate for high level sound, In proceedings of ASME 2015 Pressure Vessels and Piping Conference Volume 4: Fluid-Structure Interaction.
- [14] A. Mohany, D. Arthurs, M. Boldu, M. Hassan, S. Ziada, Numerical and experimental investigation of flow-acoustic resonance of side-by-side cylinders in a duct, *Journal of Fluids and Structures*, 48, 2014, p.316-331.
- [15] M. Mori, T. Masumto, K. Ishihara, Numerical simulation of high level sound generated in boiler tube bank duct, *International Journal of Engineering and Applied Sciences*, 5 (1), 2018, p.19-24.
- [16] F. L. Eisinger, R. E. Sullivan, Suppression of acoustic waves in steam generator and heat exchanger tube banks, *Journal of Pressure Vessel Technology*, 125 (2), 2003, p.221-227.
- [17] P. A. Feenstra, D. S. Weaver, F. L. Eisinger, Acoustic resonance in a staggered tube array: Tube response and the effect of baffles, *Journal of Fluids and Structures*, 21 (1), 2005, p.89-101.
- [18] H. Hamakawa, H. Miyagi, E. Nishida, T. Fukano, Effect of small cavities in in-line tube banks on vortex shedding, *Transactions of the Japan Society of Mechanical Engineers, Part B*, 76 (764), 2010, p.580-587.
- [19] U. Ingard, On the theory and design of acoustic resonators, *The Journal of the Acoustical Society of America*, 25, 1953, p.1037-1045.
- [20] T. H. Melling, The acoustic impedance of perforates at medium and high sound pressure levels, *Journal of Sound and Vibration*, 29 (1), 1973, p.1-65.
- [21] K. Sakagami, M. Morimoto, M. Yairi, A. Minemura, A pilot study on improving the absorptivity of a thick microperforated panel absorber, *Applied Acoustics*, 69(2), 2008, p.179-182.
- [22] C. Lawn, The acoustic impedance of perforated plates under various flow conditions relating to combustion chamber liners, *Applied Acoustics*, 106, 2016, p.144-154.
- [23] K. H. Kim, G. H. Yoon, Absorption performance optimization of perforated plate using multiple-sized holes and a porous separating partition, *Applied Acoustics*, 120, 2017, p.21-33.
- [24] K. Ishihara, Study on a countermeasure for high level sound generated from boiler tube bank duct using walls made of perforated plate (Grasp critical aperture ratio and influence of cavity volume on suppression effect) , *Transactions of the Japan Society of Mechanical Engineers*, 83 (848), 2017, p.456.
- [25] O. Inoue, M. Mori, N. Hatakeyama, Control of aeolian tones radiated from a circular cylinder in a uniform flow, *Physics of Fluids*, 15(6), 2003, p.1424.
- [26] M. Mori, T. Masumto, K. Ishihara, Study on acoustic and flow induced noise characteristics of t-shaped pipe with square cross-section, *Advances in Applied Acoustics*, 5, 2016, p.10-17.
- [27] R. Mankbadi, S-C. Lo, A. Lyrintzis, V. Golubev, Y. Dewan and K. Kurbatskii, Hybrid LES-RANS simulations of a jet impinging on a flat plate, *International Journal of Aeroacoustics*, 15(4-5), 2016, p. 535-553.
- [28] A. D. Pierce, *Acoustics: An introduction to its physical principles and applications*, McGraw-Hill, New York.
- [29] K. Ishihara, S. Kudo, T. Masumoto, M. Mori, Study on acoustic natural frequency and its mode of one dimensional sound field partitioned by perforated plate, *Transactions of the Japan Society of Mechanical Engineers*, 84 (857), 2018, p.365.